Materials Science and Engineering, B19 (1993) 129–134

Superconductivity in alkali-intercalated C_{60}

M. A. Schlüter, M. Lannoo*, M. Needels** and G. A. Baraff
AT&T Bell Laboratories, Murray Hill, NJ 07974 (USA)

D. Tomanék
Department of Physics and Astronomy, Michigan State University, East Lansing, MI 48823 (USA)

Abstract

Superconductivity observed in alkali-intercalated, solid C_{60} can be explained on the basis of conventional Bardeen–Cooper–Schrieffer theory. Intramolecular Jahn–Teller-type vibrations with high frequencies couple to conduction electrons in C_{60} π orbitals with strength V. The density of these states (N) is determined by the relatively weak intermolecular coupling. This results in a real space factorization of the coupling parameter $\lambda = NV$, which has several experimental consequences. We present detailed calculations that lead to this picture and compare these with existing experiments.

1. Introduction

The discovery of superconductivity [1] in face-centered cubic (f.c.c.) alkali-intercalated A_3C_{60} compounds (A≡K, Rb, Cs) with superconducting temperature T_c values exceeding 30 K has created considerable excitement. In this article are presented the results of detailed studies of the electronic and vibronic properties of A_3C_{60} and their coupling to each other [2–4]. We find that standard Bardeen–Cooper–Schrieffer (BCS)-type coupling to molecular vibrations can well account for all the known observations.

2. Electronic states in A_3C_{60}

It is convenient to view the electronic structure of A_3C_{60} as a result of a stepwise refinement of energy scales. In this context, we being with the largest scale, *i.e.* that of an isolated C_{60} molecule. The states can be classified into σ- like and π-like states revealing an insulating gap (1–2 eV) between the highest occupied molecular orbital (HOMO), mostly π-like level and the lowest unoccupied molecular orbital (LUMO), mostly π^*-like level. In the icosahedral group I_h, the HOMO is classified as a fivefold degenerate h_u level, while the LUMO is represented by a threefold degenerate t_{1u} level. Both are part of an 11-fold degenerate, $l=5$ manifold of π states (on a sphere) that is split by the icosahedral symmetry of C_{60}. The distribution of electronic charges is illustrated in Fig. 1, where the total valence electron density (Fig. 1(a)) is compared with the hypothetical charge of an electron added to the LUMO (Fig. 1(b)). The overlap between these LUMO states of two molecules on an f.c.c. lattice is emphasized in Fig. 2. The calculations were carried out following the density functional (*i.e.* local density approximation, LDA) approach, using a plane wave expansion and pseudopotentials, yielding results in close agreement with other studies [5–9]. The effect of the molecular orientation on the electronic structure of the LUMO complex has been studied recently [10]. Ignoring the details for the reasons of residual disorder, the main results of these studies are the formation of a LUMO band about 0.5 eV wide separated from the next higher band by about 0.5 eV. The two energy scales of the π–π complex about 10 eV wide and the intermolecular band dispersion about 0.5 eV wide are clearly separated, emphasizing the strong molecular nature of f.c.c. C_{60}.

Solid C_{60} intercalated with alkali atoms exhibits a rich phase diagram with both semiconducting and metallic phases [11]. We have concentrated on the (only) metallic phases of f.c.c. A_3C_{60} or A_2BC_{60}. In these phases, alkali atoms occupy the two tetrahedral (A) and the one octahedral (B) interstitials. The key question regarding the electronic structure of A_3C_{60} is whether the alkali atoms merely act as donors of electrons into the mostly rigid C_{60} LUMO complex or whether significant hybridization with these states takes place. Several independent calculations [3, 4, 12, 13] show

*Permanent address: ISEN, Lille, France.
**Permanent address: Lawrence Livermore National Laboratory, Livermore, CA, USA.

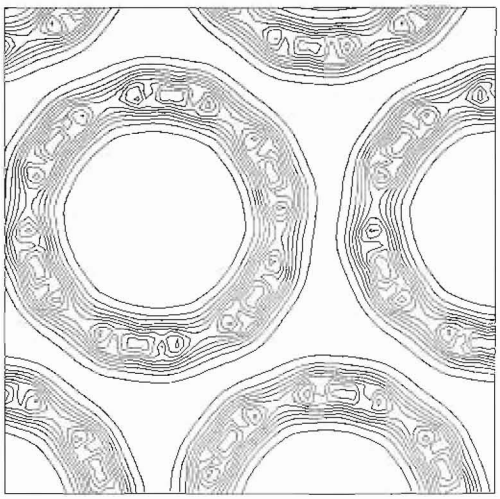

(a)

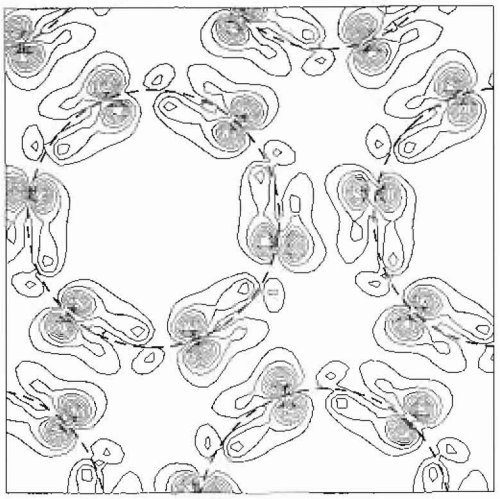

(b)

Fig. 1. Calculated electronic charge density contour plots of f.c.c. C_{60}. (a) The total valence charge density is compared with (b) the hypothetical charge density of an electron added to the LUMO.

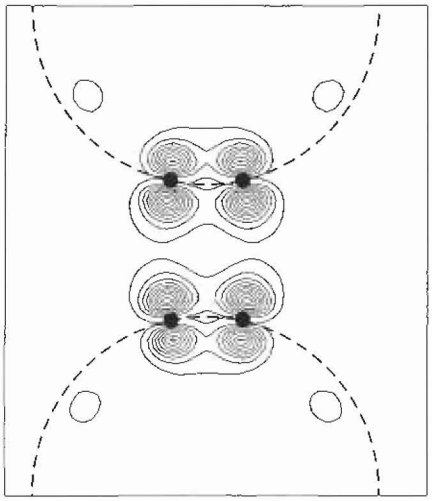

Fig. 2. Calculated charge density distribution of t_{1u} LUMO electrons, shown in a plane (close to (110)) containing two pairs of atoms on adjacent molecules.

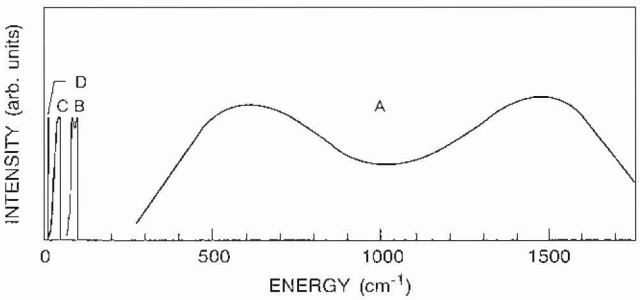

Fig. 3. Sketch of the complete vibrational spectrum of A_3C_{60}. Different groups of vibrations are emphasized. Intramolecular vibrations (A) are highest in energy, optic alkali vibrations (B) are lower, followed by acoustic intermolecular C_{60} vibrations (C) and C_{60} vibrations (D) at very low energy.

that the rigid band donor picture is essentially correct. The first alkali-derived states are found about 2 eV above the t_{1u} LUMO band. The states near the Fermi energy E_F in A_3C_{60} then have the approximate spatial distribution shown in Fig. 1(b). The bandwidth W and the density of states $N(E_F)$ to the first order depend only on the intermolecular π electron overlap, as illustrated in Fig. 2. With this picture in mind and with the purpose of conducting a study of electron–phonon interactions, we consider a simple empirical tight-binding hamiltonian [3] of the form

$$H_{TB} = \sum_{i\alpha} \epsilon_{i\alpha} C^{+}_{i\alpha} C_{i\alpha} + \sum_{i<j}^{nn} \sum_{\alpha\alpha'} t_{i\alpha j\alpha'} C^{+}_{i\alpha} C_{j\alpha'} \qquad (1)$$

where the on-site energies $\epsilon_{i\alpha}$ and the nearest-neighbor hopping integrals $t_{i\alpha,j\alpha'}$ are empirically determined parameters [13]. The scaling of these parameters with distance is an important question. Our fits to LDA results indicate a d^{-3} dependence of $t_{pp\pi}$ and a d^{-2} dependence of all the other hopping integrals. The intermolecular distance dependence of t is empirically determined from the superconductivity results to be about $d^{-2.7}$.

3. Vibrational states in A_3C_{60}

As for the electronic states, it is also instructive to subdivide the vibrations of A_3C_{60} into individual groups reflecting the molecular nature of the compound. In Fig. 3, a sketch of the full vibrational spectrum is shown. The highest frequency band (A) is due to intramolecular vibrations of C_{60}. Neutron [14] and Raman [15–18] studies have been carried out. The Raman studies of these modes are of particular interest to us, since the symmetry selection rules are the same as those that

couple to the conduction electrons in the t_{1u} LUMO. These are two symmetric, onefold degenerate A_{1g} modes and eight fivefold degenerate H_g modes. In our work, we have employed four different approximate descriptions of these vibrations. These are a Keating-type model [19] with two parameters describing the nearest-neighbor bond stretch (α) and bond bend (β) forces. (We used two different β/α ratios (0.1 and 0.3).) We further use the bond charge model developed by Weber [20] for diamond and extended to graphite and C_{60} by Onida and Benedek [21]. The fourth vibrational model we used is based on the MNDO empirical electronic structure method, with the results described in ref. 2. The average deviations from the experiment results range from about 3% to about 10%, with the empirical bond charge model giving the best overall agreement [13].

When C_{60} is condensed into an A_3C_{60} solid, additional vibrational degrees of freedom appear at finite frequencies. Here, we make no particular effort to describe quantitatively vibrations other than the intramolecular modes. As will become evident in the next section, superconductivity coupling to electrons in the t_{1u} LUMO derived band is dominated by these intramolecular modes. Coupling to the low frequency modes may affect the normal state resistivity.

4. Electron–phonon coupling in A_3C_{60}

In the BCS theory of superconductivity, the dimensionless electron–phonon coupling constant is given by

$$\lambda = \frac{2}{N(0)} \sum_{p,q} \frac{1}{2K_p(q)} \sum_{\substack{nk \\ n'k'}} |I_{nk,n'k'}(p,q)|^2 \delta(\epsilon_{nk}) \delta(\epsilon_{n'k'}) \qquad (2)$$

where ϵ_{nk} is the energy of the electronic Bloch state of band n with wavevector k, the delta functions ensure the sum to be restricted to the Fermi surface, $K_p(q) = M\omega_p^2(q)$ is the force constant of the pth phonon with wavevector q and $I_{nk,n'k'}(p,q)$ is the electron–phonon matrix element, linear in the phonon normal mode amplitudes. $N(0)$ is the density of states at the Fermi level per spin orientation. We now use a tight-binding representation for the Bloch states and we find that the derivative of an atomic hopping matrix element is calculated with respect to the motion of an atom at site τ. As pointed out earlier, this gradient matrix element is proportional to the original matrix element itself. This observation is extremely useful in a molecular crystal with significantly different energy scales. It permits us to neglect all contributions except those that modulate the strong intramolecular π–π overlap of the t_{1u} states. In this limit of $t_{inter}/t_{intra} \to 0$, one obtains

$$\lambda = N(0)\, V = N(0) \sum_p V_p = N(0) \sum_{p,\mu} \frac{\mathrm{Trace}(I^2)_{p,\mu}}{9M\omega_p^2} \qquad (3)$$

where the trace corresponds to the (3×3) matrix in the t_{1u} subspace and summations of p and μ are over the normal modes p of an isolated C_{60} with their degeneracy index μ.

Using the different electronic structure models and the different phonon models, we can now evaluate numerically

$$V = \sum_p V_p$$

Some results [13] are illustrated in Fig. 4. In the limit $t_{inter}/t_{intra} \to 0$, which we have discussed so far, no $q = k - k'$ dependence of the scattering exists. For the Jahn–Teller-type, symmetry-lowering H_g modes, the scattering is thus interband (off-diagonal in the t_{1u} LUMO manifold) on an individual C_{60} molecule. The coupling to the A_g symmetric modes is diagonal in the t_{1u} space and, therefore, does not scatter on an individual molecule. The $q = 0$ limit corresponds simply to an overall shift, as also pointed out in ref. 2. However, the modes can scatter between molecules for a finite t_{inter} and a finite q. In this case, the scattering strength would again be given by the strong t_{intra}. However, for finite doping, such as in A_3 C_{60}, the intermolecular potential produced by an A_g mode with $q \neq 0$ is likely to be screened out, effectively eliminating the contri-

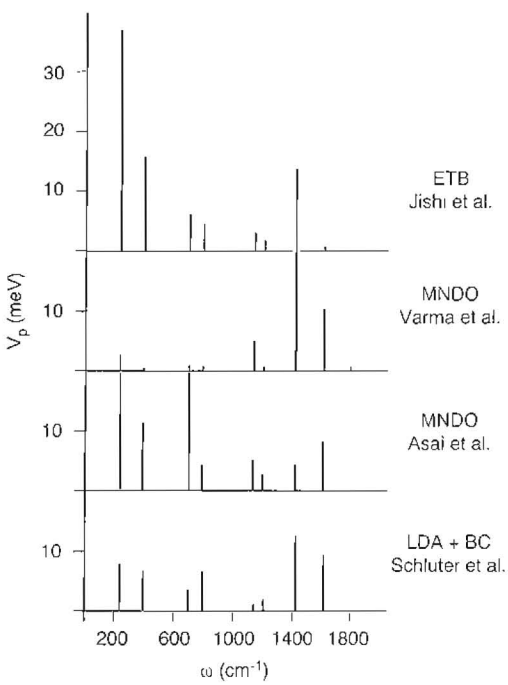

Fig. 4. Selected results for the spectral distribution of coupling strength V. Our results are obtained with the bond charge phonon model and LDA frozen phonon calculations [13].

butions of A_g modes to the electron–phonon coupling parameter in the metallic compound.

Equation (3) shows that the dimensionless coupling constant is proportional to the density of states $N(0)$ of electrons at the Fermi level E_F. Although this quantity in principle should be available from calculations and/or experiments, in practice, the situation is still unclear. On the theoretical side, the problems are mainly due to uncertainties and disorder in the orientational arrangement of C_{60} molecules [22]. Most calculations [3, 9, 10], in reasonable agreement with each other result in an average of $N(0) \approx 6$ states per eV per spin per C_{60}. On the experimental side, large variations exist in reported estimates for $N(0)$. Photoemission data [23] are interpreted to give small values, *i.e.* $N(0) \approx 1$–2. Difficulties here are associated with hole lifetime effects and/or surface sensitivity. Susceptibility measurements [24] suggest values in the range $N(0) \approx 10$–15, while nuclear magnetic resonance data [25] suggest even larger values of $N(0) \gtrsim 20$. The difficulties here are associated with extracting 'bare' density of states values in the presence of interactions and disorder. The questions are largely unsettled at this time and we have to consider reasonable ranges of $N(0)$.

5. Superconductivity

The complete theory of superconductivity has been given by Eliashberg with an approximate, explicit formula for T_c proposed by McMillan, which we have successfully tested by numerically solving Eliashberg's equation. McMillans' T_c is given by

$$T_c = \frac{\hbar\omega_{\log}}{1.2K_B} \exp\left\{\frac{-1.04(1+\lambda)}{\lambda - \mu^* - 0.62\lambda\mu^*}\right\} \tag{4}$$

where the logarithmically averaged phonon frequency $\omega_{\log}$ is given by

$$\ln \omega_{\log} = \frac{1}{\lambda} \sum_p \lambda_p \ln \omega_p \tag{5}$$

with

$$\lambda = \sum_p \lambda_p$$

Values for $\omega_{\log}$ are remarkably constant for the different phonon models [13] and, typically, are of the order of 800–1000 cm^{-1} or 1150–1450 K.

The effective Coulomb interaction μ^* is reduced from the full Coulomb repulsion μ by retardation. The effectiveness of retardation has been questioned [26] for C_{60} molecular solids on the grounds that the bandwith W for intermolecular hopping is comparable with $\hbar\omega_{\log}$. However, it is important to realize that the electronic structure of A_3C_{60} is strongly molecular only for the valence states and the first few conduction bands. Here, simple spherical atom models give strong retardation [27]. Higher-lying states intermix with the alkali states and are truly extended throughout the solid. Therefore, Coulomb scattering into these higher lying states allows electrons to hop off the C_{60} molecules at a much faster rate than that given by W. Thus, we believe that the Coulomb repulsion in A_3C_{60} is fairly standard.

It is clear that, with all the uncertainties in $N(0)$, V and μ^*, T_c cannot be reliably calculated. However, the observed T_c values can be explained well with parameters within the discussed range. For instance, for $\hbar\omega_{\log} \approx 1400$ K, as obtained from the bond charge model, $V \approx 50$ meV, which is about the calculated LDA value, an average $N(0) \approx 14$ and $\mu^* \approx 0.2$, one obtains $T_c \approx 20$ K, which is the observed T_c for K_3C_{60}. The important questions are whether or not these estimates sensibly explain observed trends and whether or not the overall picture is consistent with all experiments.

It has been noted earlier [28] that T_c varies monotonically with the A_3C_{60} lattice constants upon chemical alkali substitution. The molecular nature of A_3C_{60} 'factors' all quantities in real space. The electron–phonon coupling matrix element V and the prefactor $\hbar\omega_{\log}$ are intramolecular quantities of C_{60} and should be invariant. If we also assume μ^* to be constant to the first order, only the density of states $N(0)$ varies from compound to compound.

In Fig. 5 we show how this simple argument used with the selected values given above and a distance scaling t^{-n} with $n = 2.7$ explains precisely all the observed trends. The effect of chemical pressure is fully equivalent to mechanical pressure. Also shown in Fig. 5 are experimental results [29–31] obtained by applying hydrostatic pressure to K_3C_{60} and to Rb_3C_{60}. The results follow the same curve. This shows unambiguously that there is no alkali isotope effect.

The situation is drastically different for carbon isotope substitution. For the model developed here and with $\mu^* \approx 0.2$, we expect a reduction of α from 0.5 to 0.29. This is in excellent agreement with recent measurements by Ramirez *et al.* [32], which indicate that $\alpha = 0.37 \pm 0.05$. However, larger values of $\alpha > 1$ have also been reported [33].

The coupling of the Jahn–Teller-type modes to conduction electrons modifies these modes themselves. The self-energy can be expressed in a phonon linewidth and a frequency shift. Details are discussed in ref. 13. We observed significant phonon linewidth broadening. Particularly affected are the higher frequency modes, owing to the extra ω_p^2 factor. These results can be compared with Raman [15, 17–18] and neutron [14] scattering data, contrasting the insulating C_{60} and A_6C_{60} phases with the metallic A_3C_{60} phase.

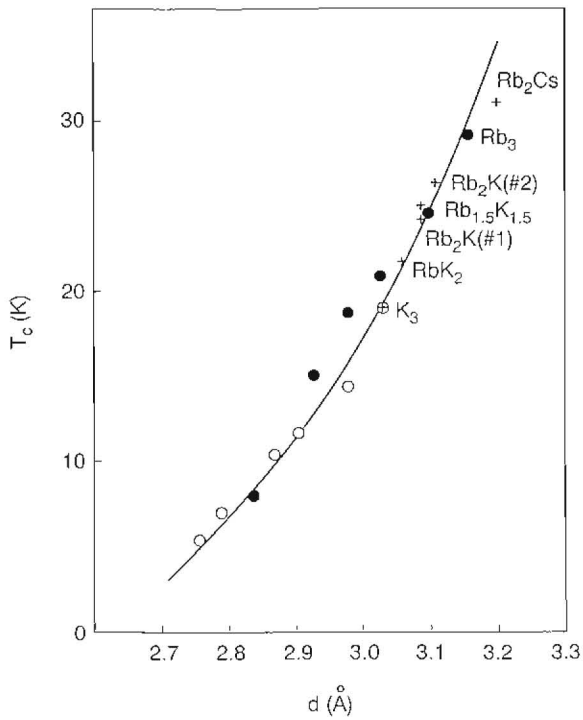

Fig. 5. Experimentally observed variation in T_c with lattice constant variations, converted here into an approximate surface distance between C_{60} molecules. Shown are the data for chemically substituted compounds (+) [28] and those obtained from K_3C_{60} (○) and Rb_3C_{60} (●) via mechanical pressure [31]. The full line is the calculated variation of T_c using McMillan's formula and the parameters discussed in the text.

In the case of Raman scattering, the (dispersionless) intramolecular modes are probed near $q \approx 0$. In a perfect crystal, the continuum of t_{1u}-derived electronic states near E_F couples to these modes for $E(k) = \omega_\rho$ near k_F, which is much larger. However, as stated earlier [27], there is considerable disorder (in particular orientational) in these materials, which should destroy q conservation and allow for Raman scattering to probe the electron–phonon coupling.

We summarize the scenario developed here for superconductivity in A_3C_{60}. The parameters are as follows: relatively high energy phonons with $\hbar\omega_{\log} \approx 1400$ K couple with a weak-to-intermediate length of $\lambda \approx 0.73$, subject to a reasonably large Coulomb repulsion of $\mu^* \gtrsim 0.2$, to yield T_c near 20 K for K_3C_{60}. We are thus not in the strong coupling limit and expect the BCS value of $2\Delta \approx 3.5kT_c$ for the superconducting gap and a coherence length of

$$\xi_0 = \frac{1}{\pi}\frac{\hbar V_F}{\Delta} \approx 130 \text{ Å}$$

Nuclear magnetic resonance and optical data seem to indicate a BCS gap value, while point contact tunnelling [34] yields larger values. Coherence lengths of about 150 Å have been inferred from H_{c2} measurements [35].

Can we use what we have learned here and extrapolate to new, hypothetical materials? If one could hole-dope C_{60}, calculations would show a T_c value in the same range as that for the electron-doped case. Similar studies for the next higher conduction band complexes (threefold t_{1g} and threefold t_{2u}) yield values for T_c in the same regime, which may be of relevance of the recently discovered Ca-intercalated materials [36].

The parameter V derives some of its contributions from coupling to lower energy radial or transverse modes. These modes couple to π-like electrons only for curved geometries. In fact, in graphite, there is no first-order coupling to transverse modes for symmetry reasons, which we suggested [3] to be the reason why T_c is much lower in intercalated graphite. Reversing the argument, we may increase T_c if we find a highly symmetric molecule (with high electronic degeneracies) with a larger curvature than that of C_{60}. We have studied the hypothetical C_{20} molecule (only pentagons) which is insulating in its + charge state. The coupling V is found to be indeed about 1.5 times stronger than that in C_{60}. Chemically, however, the atoms have near-perfect sp^3 bond angles and the 'lone pairs' probably make C_{20} highly reactive.

6. Conclusions

We have examined the electronic and vibrational structure of A_3C_{60} compounds in detail and found by direct calculations that the Jahn–Teller-type intramolecular modes efficiently couple to the conduction electrons induced by alkali intercalation. This coupling (V) is largely an isolated molecule property and can be derived from Jahn–Teller-type studies. The hopping between the molecules is the second important ingredient in that it determines the kinetic energy or the density of states (N) of conduction electrons. The dimensionless BCS coupling parameter $\lambda = NV$ is then factorized in real space, a picture which is precisely confirmed by several experiments, such as studies of chemical or mechanical pressure affecting T_c and vibrational linewidth studies in Raman or neutron experiments. Moreover, the absence of any alkali isotope effect and the observation of a strong effect upon carbon isotope substitution can be quantitatively explained.

Acknowledgments

We thank W. Zhang and Y. Wang for assistance with numerical calculations and many of our colleagues for discussions of their results.

References

1 A. F. Hebard, M. J. Rosseinsky, R. C. Haddon, D. W. Murphy, S. H. Glarum, T. T. M. Palstra, A. P. Ramirez and A. R. Kortan, *Nature, 350* (1991) 600.
2 C. M. Varma, J. Zaanen and K. Raghavachari, *Science, 254* (1991) 989.
3 M. A. Schlüter, M. Lannoo, M. Needels, G. A. Baraff and D. Tomanek, *Phys. Rev. Lett., 68* (1992) 526.
4 I. I. Mazin, S. N. Rashkeev, V. P. Antropov, O. Jepsen, A. I. Lichtenstein and O. K. Andersen, *Phys. Rev. B, 45* (1992) 5114.
5 J. H. Weaver, J. L. Martinsw, T. Komeda, Y. Chen, T. R. Ohno, G. H. Kroll, T. Troullier, R. E. Hauffer and R. E. Smalley, *Phys. Rev. Lett., 66* (1991) 1741.
6 Q. Zhang, J. Y. Yi and J. Berhnolc, *Phys. Rev. Lett., 66* (1991) 2633.
7 S. Saito and A. Oshiyama, *Phys. Rev. Lett., 66* (1991) 2637.
8 B. P. Feuston, W. Andreoni, M. Parrinello and E. Clementi, *Phys. Rev. B, 44* (1991) 4056.
9 N. Troullier and J. L. Martins, to be published.
10 S. Satpathy, V. P. Antropov, O. K. Andersen, O. Jepsen, O. Gunnarsson and A. I. Lichtenstein, *Phys. Rev.*, in press.
11 D. W. Murphy, M. J. Rosseinsky, R. M. Fleming, R. Tycko, A. P. Ramirez, R. C. Haddon, T. Siegrist, G. Dabbagh, J. C. Tully and R. E. Walstedt, *J. Phys. Chem. Sol.*, in press.
12 J. L. Martins and N. Troullier, *Phys. Rev.* in press.
13 M. Schlüter, M. Lannoo, M. Needels, G. A. Baraff, D. Tomanek, *J. Phys. Chem. Sol.*, in press.
14 K. Prassides, J. Tomkinson, C. Christides, M. J. Rosseinsky, D. W. Murphy and R. C. Haddon, *Nature, 354* (1991) 462.
15 S. J. Duclos, R. C. Haddon, S. H. Glarum, A. F. Hebard and K. B. Lyons, *Science, 254* (1991) 1625.
16 D. S. Bethune, G. Meijer, W. C. Tang, H. J. Rosen, W. G. Golden, H. Seki, C. A. Brown and M. S. deVries, *Chem. Phys. Lett., 179* (1991) 181.
17 M. G. Mitch, S. J. Chase and J. S. Lannin, *Phys. Rev. Lett., 68* (1992) 883.
18 P. Zhou, K. Wang, A. M. Rao, P. C. Eklund, G. Dresselhaus and M. S. Dresselhaus, *Phys. Rev.*, in press.
19 R. Martin, *Phys. Rev. B, 4* (1970) 4005.
20 W. Weber, *Phys. Rev. B, 15* (1977) 4789.
21 G. Onida and G. Benedek, *Europhys. Lett.*, in press.
22 M. P. Gelfand and J. P. Lu, *Phys. Rev. Lett., 68* (1992) 1050.
23 C. T. Chen, L. H. Tjeng, P. Rudolf, G. Meigs, J. E. Rowe, J. Chen, J. P. McCauley, A. B. Smith, A. R. McGhie, W. J. Romanow and E. Plummer, *Nature, 352* (1991) 603.
24 A. P. Ramirez, M. J. Rosseinsky, D. W. Murphy and R. C. Haddon, *Phys. Rev. Lett., 69* (1992) 1687.
25 R. Tycko, G. Dabbagh, M. J. Rosseinsky, D. W. Murphy, R. M. Fleming, A. P. Ramirez and J. C. Tully, *Science, 253* (1991) 884.
26 S. Chakravarty, S. Khlebnikov and S. Kivelson, *Phys. Rev. Lett., 69* (1992) 212C.
27 M. Schlüter, M. Lannoo, M. Needels, G. A. Baraff and D. Tomanek, *Phys. Rev. Lett., 69* (1992) 213C.
28 R. M. Fleming, A. P. Ramirez, M. J. Rosseinsky, D. W. Murphy, R. C. Haddon, S. M. Zahurak and A. V. Makhija, *Nature, 352* (1991) 787.
29 J. E. Schirber, D. L. Overmyer, H. H. Wang, J. M. Williams, D. D. Carlson, A. M. Kini, M. J. Pellin, U. Welp and W.-K. Kwok, *Physica C, 178* (1991) 137.
30 G. Sparn, J. D. Thompson, S.-M. Huang, R. B. Kaner, F. Diederich, R. L. Whetten, G. Gruner and K. Holczer, *Science, 252* (1991) 1829.
31 O. Zhou, G. B. M. Vaughn, Q. Zhu, J. E. Fischer, P. A. Heiney, M. Coustel, J. P. McCauley and A. B. Smith, preprint.
32 A. P. Ramirez, A. R. Kortan, M. J. Rosseinsky, S. J. Duclos, A. M. Mujsce, R. C. Haddon, D. W. Murphy, A. V. Makhija, S. M. Zahurak and K. B. Lyons, *Phys. Rev. Lett., 68* (1992) 1058.
33 T. W. Ebbesen, J. S. Tsai, K. Tanigaki, J. Tabuchi, Y. Shimakawa, Y. Kubo, I. Hirosawa and J. Mizuki, *Nature, 355* (1992) 620.
34 Z. Zhang, C.-C. Chen, S. P. Kelty, H. Dai, C. M. Lieber, *Nature, 253* (1991) 333.
35 T. T. M. Palstra, R. C. Haddon, A. F. Hebard and J. Zaanen, *J. Phys. Rev. Lett., 68* (1992) 1054.
36 A. R. Kortan, N. Kopylov, S. H. Glarum, E. M. Gyorgy, A. P. Ramirez, R. M. Fleming, F. A. Thiel and R. C. Haddon, *Nature, 355* (1992) 529.